Bone 45 (2009) 84–90

Contents lists available at ScienceDirect

Bone

journal homepage: www.elsevier.com/locate/bone

Determining the elastic modulus of mouse cortical bone using electronic speckle pattern interferometry (ESPI) and micro computed tomography: A new approach for characterizing small-bone material properties ☆

Netta Lev-Tov Chattah [a,*], Amnon Sharir [b], Steve Weiner [a], Ron Shahar [b]

[a] Department of Structural Biology, Weizmann Institute of Science, 76100 Rehovot, Israel
[b] Koret School of Veterinary Medicine, The Hebrew University of Jerusalem, Rehovot, Israel

ARTICLE INFO

Article history:
Received 27 January 2009
Revised 9 March 2009
Accepted 11 March 2009
Available online 28 March 2009

Edited by: T. Einhorn

Keywords:
Elastic modulus
Biomechanical testing
Electronic speckle pattern interferometry
Mouse
Femur

ABSTRACT

Mice phenotypes are invaluable for understanding bone formation and function, as well as bone disease. The elastic modulus is an important property of bones that can provide insights into bone quality. The determination of the elastic modulus of mouse cortical bone is complicated by the small dimensions of the bones. Whole bone bending tests are known to under estimate the elastic modulus compared to nanoindentation tests. The latter however provides information on extremely localized areas that do not necessarily correspond to the bulk elastic modulus under compression.

This study presents a novel method for determining the bulk or effective elastic modulus of mouse cortical bone using the femur. We use Electronic Speckle Pattern Interferometry (ESPI), an optical method that enables the measurement of displacements on the bone surface, as it is compressed under water. This data is combined with geometric information obtained from micro-CT to calculate the elastic modulus. Roughly tubular cortical bone segments (2 mm) were cut from the diaphyses of femora of four week old C57BL/6 (B6) female mice and compressed axially using a mechanical tension–compression device. Displacements in the loading direction were mapped on the bone surface after loading the specimen. A linear regression of the displacement vs. axial-position enabled the calculation of the effective strain. Effective stress was calculated using force (N) data from the system's load cell and the mean cross-sectional area of the sample as determined by micro-CT. The effective elastic modulus (E) was calculated from the stress to strain ratio. The method was shown to be accurate and precise using a standard material machined to similar dimensions as those of the mouse femoral segments.

Diaphyses of mouse femora were shown to have mean elastic moduli of 10.4 ± 0.9 GPa for femora frozen for eight months, 8.6 ± 1.4 GPa for femora frozen for two weeks and 8.9 ± 1.1 GPa for the fresh femora. These values are much higher than those measured using three-point bending, and lower than values reported in the literature based on nanoindentation tests from mice bones of the same age. We show that this method can be used to accurately and precisely measure the effective elastic modulus of mouse cortical bone.

Introduction

Mice are invaluable animal models for understanding genetic mechanisms controlling the processes of bone formation, growth, physiology and disease, as well as for evaluating novel therapies [1,2,12,13,16–20,22,28]. Detailed characterization of the bone phenotype entails a multilevel description of bone geometry, architecture, material makeup, mechanical behavior and material properties.

Stiffness is an important mechanical property of the bone material and greatly depends on mineralization and porosity [9,11]. The *intrinsic* stiffness of the bone is quantified by the elastic or Young's modulus, an inherent property of the bone material [40]. The elastic modulus is a fundamental determinant of bone's mechanical behavior. However, the small size of mice bones complicates the task of determining their elastic moduli. The importance and complexity of this issue is manifested by the large number of papers describing various methods proposed to quantitatively measure elastic modulus of mice bones [29,32,36–39,42–43]. Here we present a new approach for determining the effective or bulk elastic modulus

☆ This research was funded by Kekst Family Center for Medical Genetics at the Weizmann Institute of Science. S. W. is the incumbent of the Dr. Walter and Dr. Trude Burchardt Professorial Chair of Structural Biology.

* Corresponding author. Fax: +972 8 9344136.
E-mail address: Netta.Lev-tov-chattah@weizmann.ac.il (N.L.-T. Chattah).

8756-3282/$ – see front matter © 2009 Elsevier Inc. All rights reserved.
doi:10.1016/j.bone.2009.03.664

of mouse cortical bone using the femur. In this method mechanical testing is preformed in a manner similar in principle to the way a bone cube obtained from a larger animal would be tested in standard mechanical compression.

Bone is a graded, hierarchical and anisotropic material. Its elastic modulus thus varies at different length scales and depending upon the direction of force applied [9]. Mechanical tests employed to determine the bulk mechanical properties of bone use relatively large machined bone samples to measure the elastic modulus directly by standard compression and tension testing. Mice bones are minute and are therefore usually tested as whole entities. Two main types of bending tests, namely three-point bending and four point bending are used to determine the effective elastic modulus of whole mouse long bones [7,12,14–16,22,27,32,43]. By far the most common test is three-point bending [6,34]. Calculation of the elastic modulus in bending tests is based on the Euler–Bernoulli *beam theory*, derived from the linear theory of elasticity [34]. The main underlying assumptions of this approach are that the tested sample is isotropic, has uniform cylindrical geometry and does not undergo shear stresses during loading. Bone is not isotropic, and its geometry is irregular. Furthermore, bending tests are associated with some degree of shear, and local ring-type deformations occur where the supports and loading prong contact the bone; especially in bones with a thin cortex [32,39,41]. Significant errors are thus introduced when measuring the effective elastic modulus using bending tests of whole bones. The result is that the modulus is usually markedly underestimated [36,39,41]. Recently finite element models (FEMs) have been used to provide correction factors in order to more accurately predict the elastic modulus of mice bones measured by three-point bending [41]. These models are themselves based on various approximations and the corrections are still sub-optimal.

Another widely used approach is nanoindentation. However this method measures the elastic modulus at the nanoscale and is therefore sensitive to the local microstructure [3,8,17,20,26,36,38]. The measurements involve some plastic deformation in addition to elastic deformation and testing is usually preformed on a dry [3,17,38] or semi-hydrated samples [26], increasing the stiffness of the bone material [30]. Measurements of the elastic modulus of mouse cortical bone using nanoindentation produce values around 26–31 GPa [3,8,26,36]. Silva et al. [36] and Chen et al. [8] noted the marked discrepancy between elastic moduli obtained using bending tests and nanoindentation tests, with the results of bending tests being significantly lower than those obtained by nanoindentation.

Ultrasonic techniques can also be used to provide data regarding the mechanical properties of bulk bone material, but are an indirect measurement of the elastic modulus. Somerville et al. [37] have estimated the elastic modulus of mature B6 mice tibia as 22.3 ± 2.6 GPa for males and 23.2 ± 2.8 GPa for females. Recently Raum et al. [29] used a method which combines scanning acoustic microscopy and synchrotron-radiation micro-CT to determine the transverse bulk elastic modulus of 5.5 month old mice femora (B6 and C3H). Their results (16.1 ± 1.8 GPa and 22.4 ± 1.9 GPa respectively) are roughly comparable to those using nanoindentation.

Electronic speckle pattern interferometry (ESPI) is a non-contact optical metrology method which enables direct measurements of the displacements on the surface of mineralized tissues during mechanical loading [4,5,21,33,45–47]. It is both precise and accurate for determining the effective elastic modulus of cortical bone cubes submerged in water [33]. The method is extremely sensitive and allows detection of displacements at the nanometer level in millimeter-sized specimens [33,45,46]. In this paper we take advantage of the tubular-shaped, midshaft diaphysis of the mouse femur in a section whose cortical cross-sectional area is nearly uniform along the axial direction, and show that ESPI can be used for accurately and precisely determining the effective elastic modulus of this millimeter-sized, cortical bone segment.

Materials and methods

Mid-diaphyseal segments of mice femora, two mm-long, were incrementally loaded in compression under water. Surface displacements were measured in the direction of compression (axial) using ESPI. The resulting effective strain in the loading direction was determined from the displacements, allowing calculation of the effective elastic modulus.

Bone sample preparation

Sixteen four week old, C57 BL/6 (B6), female mice, purchased from Harlan Biotech Israel Ltd. were anesthetized with isoflurane-soaked gauze in a sealed chamber, and sacrificed by cervical dislocation. The study was approved by the institutional animal care and use committee.

The average weight of the mice was 12.03 ± 0.77 g. The left and right femora were carefully excised and manually cleaned of soft tissues. A cortical mid-diaphyseal section, starting just distal to the third trochanter and extending 2 mm distally was cut using a water-cooled, slow diamond saw (Buehler). Six segments were damaged during the cutting process and could not be tested. The prepared segments were scanned by micro-CT (eXplore locus SP, General Electric, USA) and then wrapped in saline-soaked gauze until mechanical testing was performed. A total of 23 femoral segments were arbitrarily separated into three groups, stored in different manners prior to testing. One group consisted of twelve femora frozen at −20 °C for eight months, a second group consisted of five femora frozen at −20 °C for two weeks and a third group of six femora was tested immediately after harvesting.

The right femora of five additional four week old, B6, female mice were harvested for whole-bone three-point bending tests, and were frozen for two months at −20 °C prior to testing. Whole femora of this group were scanned by micro-CT, then wrapped in saline-soaked gauze and stored at 4 °C until testing.

Prior to testing, the frozen femora and/or femoral segments were slowly thawed at room temperature. During the different stages of sample preparation the bones were kept moist and refrigerated at 4 °C.

Micro-CT structural analysis

Five whole femora and 23 femoral segments were scanned using a micro-CT device (eXplore locus SP, General Electric, USA). Sixteen micrometer voxel-size scans were acquired. The X-ray source was set at 80 kV and 80μA. 720 projections were acquired over an angular range of 360°. The image slices were reconstructed using custom software (Microview reconstruction software, version 5.2.2). Before analysis all scans were reoriented in order to uniformly align their scan axes and anatomical position (i.e. proximal–distal, dorsal–ventral, and medial–lateral).

Whole femora: Analysis of cortical bone was performed on a 0.5 mm-long transverse section of the diaphysis of the femur (approximately 30 slices), adjacent and distal to the third trochanter (Fig. 1A). The cross-sectional moment of inertia (CSMI) was determined.

Femoral segments: Analysis of cortical bone was performed every 16 μm along the segment height (~2 mm). This scan provided the mean cross-sectional area of the segment along its length.

Mechanical testing setup and loading scheme

A thin coat of white waterproof paint was applied to the diaphyseal bone segments by spraying in order to increase the intensity of light reflected from the samples [44,45]. A thin layer (~0.5 mm) of dental composite (Z100, 3 M-ESPE) was placed on the lower (stationary)

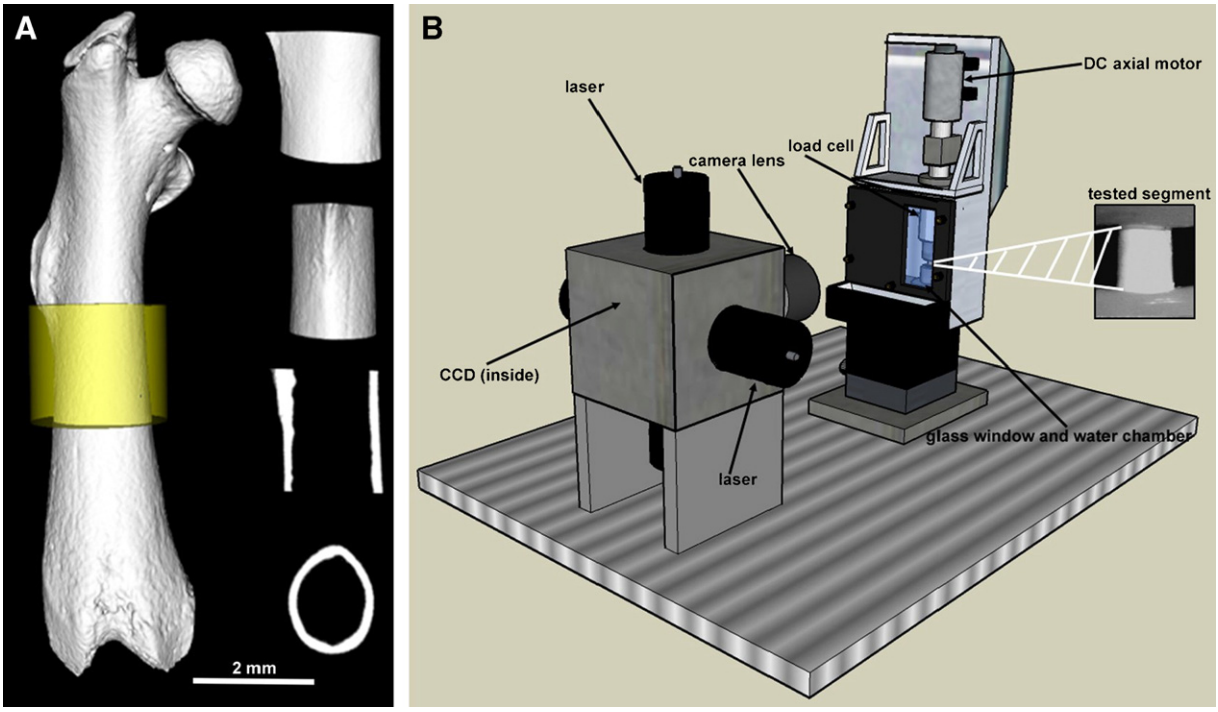

Fig. 1. (A) Micro-CT images of the whole femur (cranial view) with the 2 mm diaphyseal section of interest marked in yellow (left), to the right from top to bottom different views of a 2 mm segment: cranial view, lateral view, longitudinal cross-section, transverse cross-section. (B) ESPI Experimental setup showing the location of the tested segment [3D image by Dr. M.M. Barak (Google Skechup 7)].

anvil, and each segment was mounted such that its distal cross-section rested on the composite with its medial surface facing towards the CCD camera of the ESPI (Fig. 1B). The composite was then cured by exposure to blue light for 60 s (LITEX 682, Dentamerica CA, USA). A second layer of dental composite was placed on the upper anvil, which was then lowered until the proximal cross-section of the segment was brought into contact with the uncured composite. The dental composite, which enveloped the edge of the third trochanter, was now cured for 60 s. After the composite was cured the upper (mobile) upper anvil was lowered further, until a pre-load compression of ~3.5–4.5 N was reached. Finally, the test chamber was fitted with a high-grade glass window (BK-7 λ/10 grade) and filled with water (Fig. 1B). Water is a major component of mineralized tissues such as bones, and testing bone samples while submerged in water maintains the biomechanical properties of the bone material, known to be compromised by drying and subsequent microcracking [30,45].

Each segment was loaded axially and incrementally in compression using a custom-designed mechanical tension–compression device [33]. The upper, mobile anvil is a stainless-steel rod attached to an immersible load cell (AL311BN, I6, Honeywell-Sensotec, OH, USA) capable of measuring loads up to 120 N in tension or compression. The rod was moved by a sub-micrometer high-precision DC motor and controller (PI M-235.5DG, Physik Instrumente (PI) GmbH, Germany) in order to compress the femoral segment against the lower stationary anvil. The segments were compressed non-destructively within their elastic region, therefore allowing repeated measurements. Each experiment consisted of four sets of loading cycles in which the samples were loaded in compression in 50 successive steps of 0.5 micrometer increments of the upper anvil (25 micrometer movement in total). A 1.5 second pause was required between successive loading increments to allow for the ESPI measurements.

Force measurements were collected and stored on a computer using an A/D converter (Omega DAQP-308 PCMCIA 16-bit Analogue I/O) and further analyzed by custom-written software (National Instruments Labview v 7.0 and Matlab v 6.0). At the end of each compression set the upper anvil automatically returned to its original pre-load position. By repeating the entire loading sequence four times a robust and repeatable data set was obtained. Moreover, since each loading sequence itself was composed of 50 individual steps, each of which can be evaluated independently, the statistical robustness was further strengthened.

Upon the completion of four sets, the sample was completely unloaded, the water was drained, the test chamber was opened and the upper anvil with the composite attached to it was lifted from the sample.

ESPI optical measurements

Using a commercially available ESPI device (Q300, Dantec-Ettemeyer, Ulm, Germany) and custom-written software (Matlab v 6.0), surface displacements were recorded before and after each of the loading steps on the medial surface of the tested segments in the axial (*Y*) direction. In this method, described previously in detail [45], the rough surface of the bone is illuminated by a coherent laser light source (780 nm wave length) using a dual illumination scheme [33,45,46]. This optically rough surface is required for application of speckle interferometry techniques [45]. As coherent laser light scatters from the optically rough surface of the bone, speckles are formed due to local interference. Interference with a reference beam is imaged onto a CCD detector array. The differences between patterns of consecutive speckle images taken before and after applying the load are used to detect shifts in the phases of the speckles. These phase shifts correspond to displacements of the surface relative to a reference point selected within the region of interest, and their extent can be determined using a phase shifting algorithm combined with phase unwrapping. This technique is extremely sensitive, and it is possible to measure displacements as small as 25 nm and generate full-field displacement maps (Fig. 2).

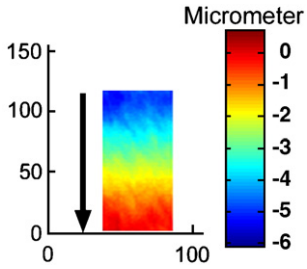

Fig. 2. *Y*-displacement map based on the mean displacements obtained from four repeated loading sequences. The black arrow points to the direction of the applied force. The axes represent the number of pixels in the region of interest (pixel size approximately 12 μm).

Elastic modulus: ESPI optical data analysis

Cumulative *Y*-direction displacement matrices were created for all four experimental sets conducted for each segment by summation of the displacement matrices measured at each of the 50 loading steps. Every cumulative matrix thus provides the total displacement (micrometers) for each pixel in the region of interest (over 5000 data points) located on the surface of the sample at the end a full cycle of 50 loading steps. Each row in the matrix provides the *Y*-displacements of pixels located at the same *Y*-position above the lower anvil. The measured displacements were nearly uniform at each *Y*-position in all experiments and in all samples tested. We could therefore represent the displacements of each row (*Y*-position) by its mean, resulting in a vector of displacements along the *Y*-direction of the sample. The displacement vs. *Y*-position relationship was plotted, and a linear regression calculated. The high R^2 values obtained (in all experiments the R^2 values were never less than 0.99) show that the displacements consistently varied linearly with the *Y*-position (see Fig. 2). The slope of this linear regression represents the effective strain of the sample in the *Y*-direction. It should be noted that while the magnitude of the measured displacements is determined relative to a reference point, the gradient measured (Y component of the strain) is absolute. The delta force between pre-load and the load reached at the end of the 50-step set was obtained from the measurements provided by the load cell. This force was divided by the mean cross-sectional area of the sample as determined by micro-CT scanning, and the resulting value was considered as the effective stress. The effective elastic modulus (E) was thereafter calculated as the ratio of the effective stress to the effective strain.

Validation

In order to validate the proposed method, three ULTEM tube samples were prepared. The tubes were made to resemble the bone segments, namely 2 mm in length, with an outer diameter of 1.26 mm and inner diameter of 1 mm. ULTEM 1000 (Acetal Polyether Imide) is an isotropic material (ULTEM 1000®, General Electric Plastics), with a known elastic modulus, reported by the manufacturer as ~3516 Mpa. The tubes were tested according to the protocol described above.

Elastic modulus: three-point bending

Five whole femora were tested in three-point bending. Biomechanical testing was performed using the same custom-designed mechanical tension–compression device described above, fitted with a custom-built three-point bending testing device. All bones were tested while fully immersed in water. Each femur was placed on two supports having rounded profiles (0.5 mm diameter) such that the supports were located equidistant from the ends of the bone, and both contacted the anterior aspect of the diaphysis. The span between the supports was 5 mm. Each bone was loaded on its posterior aspect, at the mid-distance between the bottom supports. Loading was conducted at a constant rate (200 μm/min). Force–displacement data were collected by custom-written software (Lab view 7.0) at 50 Hz. The resulting load–displacement curves were analyzed to calculate whole-bone stiffness (slope at the linear portion of the load–displacement curve). The effective elastic modulus of the cortical bone material was estimated based on beam theory which yields the following relationship:

$$E = \frac{s \cdot L^3}{48I} \quad (1)$$

where E is the effective elastic modulus (N/mm^2), S is the slope of the linear portion of the load–displacement curve (N/mm), L is the support span (mm) and I is the cross-sectional moment of inertia (mm^4) of the mid-diaphysis of the tested bone, as determined by micro-CT.

Statistical analyses

Statistical analyses were preformed using Graphpad prism 5.0 software (GraphPad, Inc. CA). Statistical significance was set at $P<0.05$. One-way-analysis-of-variance (ANOVA) was used to compare the effective elastic moduli of the tested femoral segments between the different groups, followed by a Tukey posthoc test. Elastic moduli of paired (left and right) femoral segments were compared using a paired Student's *t*-test. Spearman's rank correlation was used to examine the correlation between mouse weight and elastic modulus.

Results

Micro-CT structural analysis

Table 1 provides the mean cortical area along the length of the segments. The results show that the cortical area was uniform throughout the segment, as inferred from the small standard deviations.

Elastic modulus based on ESPI optical data analysis

Determination of the effective elastic modulus of 2 mm femoral segments of four week old B6 mice using ESPI (Table 1), shows that

Table 1
Geometric parameters of the bone segments and ESPI derived strain, stress and elastic moduli (E).

Storage	Specimen	Cortical cross-sectional area (mm^2)	Stress (MPa)	Strain (μs)	E (GPa)
		Mean (±SD)	Mean (±SD)	Mean (±SD)	Mean (±SD)
Frozen:	201R	0.40 (0.01)	50.24 (0.65)	5480 (130)	9.18 (0.11)
8 months	201L	0.40 (0.02)	53.04 (0.51)	4900 (0)	10.82 (0.10)
	202R	0.40 (0.01)	50.80 (0.79)	4750 (90)	10.70 (0.28)
	202L	0.39 (0.01)	54.97 (0.55)	5430 (40)	10.01 (0.07)
	203R	0.43 (0.01)	48.81 (0.62)	4330 (40)	11.29 (0.17)
	203L	0.41 (0.01)	54.56 (0.54)	4680 (80)	11.68 (0.29)
	204L	0.40 (0.01)	49.01 (0.52)	5580 (160)	8.70 (0.19)
	205L	0.49 (0.01)	48.60 (0.52)	4400 (70)	11.05 (0.16)
	206L	0.47 (0.01)	47.64 (0.25)	4430 (150)	11.03 (0.36)
	207L	0.47 (0.01)	49.97 (0.66)	4950 (110)	10.10 (0.14)
	209L	0.48 (0.02)	45.74 (0.43)	4280 (110)	10.71 (0.25)
	210L	0.49 (0.01)	50.74 (0.35)	5200 (120)	9.76 (0.29)
Frozen:	301R	0.46 (0.01)	49.54 (0.59)	5780 (190)	8.59 (0.21)
2 weeks	302R	0.47 (0.01)	51.66 (0.14)	5480 (150)	9.44 (0.25)
	303R	0.45 (0.02)	50.96 (0.22)	4980 (80)	10.25 (0.15)
	305R	0.40 (0.01)	52.38 (0.36)	6080 (220)	8.63 (0.26)
	306R	0.48 (0.01)	41.54 (0.24)	6930 (130)	6.00 (0.08
Fresh	302L	0.47 (0.01)	45.60 (0.18)	5750 (180)	7.94 (0.28)
	303L	0.42 (0.01)	54.34 (0.52)	6480 (180)	8.40 (0.17)
	304L	0.42 (0.01)	49.11 (0.21)	6330 (40)	7.77 (0.05)
	305L	0.47 (0.02)	42.46 (0.44)	5130 (40)	8.29 (0.09)
	306L	0.36 (0.01)	62.09 (0.34)	5900 (70)	10.52 (0.13)
	307L	0.40 (0.01)	56.64 (0.88)	5430 (110)	10.44 (0.20)

L = left femur; R = right femur.

the mean moduli calculated for the different groups were: 10.4 ± 0.9 GPa for the femora frozen for eight months, 8.6 ± 1.4 GPa for the femora frozen for two weeks and 8.9 ± 1.1 GPa for the fresh femora. A one way ANOVA ($P<0.0086$) followed by a Tukey posthoc test showed that the samples from the group frozen for eight months had a significantly higher mean elastic modulus compared to both fresh segments and those frozen for two weeks ($P<0.05$). The elastic moduli of paired left and right femoral segments of the same individual did not differ in the frozen group ($n=3$) or in the pooled fresh and recent frozen group ($N=4$) (Paired Student's t-test). No correlation was found between body weight and the calculated elastic modulus (Spearman's Rank correlation).

Validation

Table 2 shows mean elastic moduli calculated for three ULTEM tubes determined by the method described above. The table also provides a comparison with values supplied by the manufacturer based on three-point bending tests and with those determined by compression of ULTEM 2 × 2 × 2 mm cubes using the ESPI method [33]. The measured moduli of the ULTEM tubes were within 8.5% of the value reported by the manufacturer and were close to values previously reported by Shahar et al. [33]. These results indicate that the ESPI method is accurate in determining the elastic modulus of millimeter-sized, tubular-shaped geometrical specimens.

Precision

The mean elastic moduli of both bone segments and ULTEM tubes are based on averaging elastic moduli obtained from four separate incremental loading experiments for each specimen. Tables 1 and 2 show that the standard deviation between the sets is low, ranging between 0.64 and 3.53% for the bone segments and 1.14 and 1.99% for the ULTEM tubes. In the bone segments (Table 1); effective stress and strain also have low standard deviations ranging between 0.57 and 1.56% and 0 and 3.62%, respectively. These results indicate that the ESPI method is precise.

Three-point bending

The elastic moduli obtained from three-point bending tests were low compared to results by ESPI (Fig. 3 and Table 3). The mean modulus for all bones ($n=5$) was 0.88 ± 0.18 GPa.

Discussion

In this study we introduce a novel method for determining the effective elastic modulus of mice cortical bone using millimeter-sized, femoral, midshaft diaphyses segments tested in compression. The elastic modulus is determined using ESPI, an optical metrology method and is based on averaging the elastic moduli obtained by four independent experiments for each segment. We show that the ESPI method can be used to both accurately and precisely determine the effective elastic modulus of cortical bone segments by direct measurement of surface displacements during compression in the axial direction. The method was tested on four week old mice and the moduli observed were much greater than those reported in the literature for mice whole femora of the same age whose elastic moduli were determined by bending tests (Fig. 3).

Studies have shown that whole-bone bending tests used for determining of the effective elastic modulus of mouse cortical bone suffer from major methodological drawbacks as well as a disparity in testing setups and results [41]. These drawbacks are enhanced when dealing with long bones of very young mice with relatively thin cortices. It is not surprising therefore that only few studies have reported the elastic modulus for mice of such a young age using bending tests. Studies such as those conducted by van Lenthe et al. [41] have shown that the moduli determined for mice femora based on beam theory greatly underestimate the tissue modulus, especially in mice with relatively thin cortices and large midshaft diameter such as the B6 strain. The researchers used micro-finite element analysis to correct for this bias, and obtained values of 12.0 ± 1.3 GPa for 15 week old B6 mice.

The elastic moduli of mouse cortical bone determined by nanoindentation are much higher in all age groups than those obtained from bending tests [3,8,17,20,26,36,38]. Miller et al. [26] reported

Table 2
Elastic modulus of ULTEM 1000® GPa.

	Manufacturer[a]	ESPI-ULTEM tubes	ESPI-ULTEM cubes[b] ($n=10$)
Data	3.52 GPa	3.22 ± 0.06 GPa ($n=1$) 3.26 ± 0.05 GPa ($n=1$) 3.53 ± 0.06 GPa ($n=1$)	3.42 ± 0.10 GPa 3.43 ± 0.10 GPa
Mean ± SD	3.52 GPa	3.34 ± 0.14 GPa	3.43 ± 0.005 GPa

[a] GE Plastics ULTEM 1000® Data Sheet, based on three-point bending tests (no SD provided).
[b] Shahar et al. [33] based on compression tests, determined by two different calculation methods.

Table 3
Elastic modulus (E) of three-point bending tests using 5 mm support span.

Specimen no.	S (N/mm)	I (mm^4)[a]	E (GPa)
301	34	0.109	0.812
302	23	0.093	0.644
303	27	0.091	0.772
304	40	0.096	1.080
305	47	0.110	1.112

S Slope of linear portion of the load/displacement curve.
I Cross sectional moment of inertia.
[a] Based on Micro-CT data.

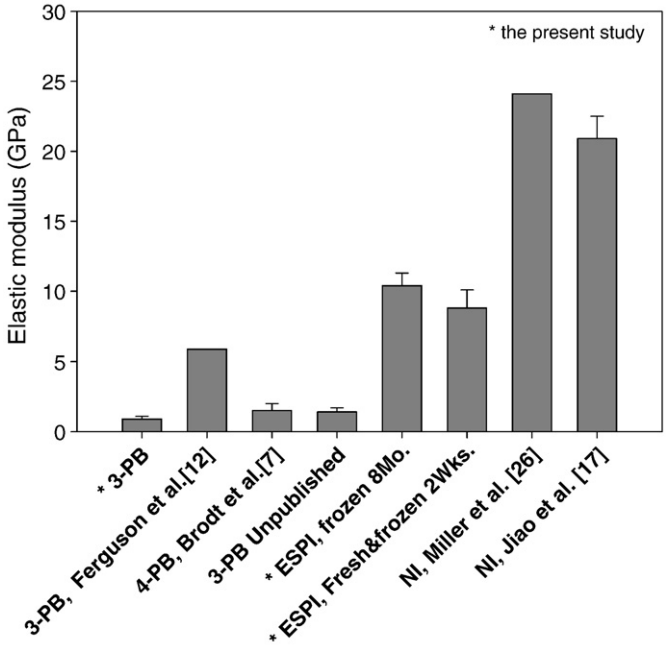

Fig. 3. Mean elastic moduli and SD (where provided) of four–five week old mice femora and tibia using different testing methods. 3-PB: three-point bending; 4-PB: four point bending; ESPI: electronic speckle pattern interferometry; NI: nanoindentation. The unpublished three-point bending study was conducted in the Laboratory of Biomechanics, School of Veterinary Medicine, Faculty of Agriculture, Hebrew University, Jerusalem Israel.

values ranging between 21 and 28 GPa for 30-day old BALB/cByJ female mice tibia, while Jiao et al. [17] report values of 20.9 ± 1.6 GPa for 4 week old C3H female tibia. The bones were hydrated before but not during the long process of testing. Somerville et al. [37] used ultrasound to determine the longitudinal bulk elastic modulus of one month old B6 mice tibia. They report 15.5 GPa for females and 17.9 GPa for males.

Fig. 3 shows that nanoindentation, three-point bending and ESPI all produce different elastic moduli for bones of more or less age-matched mice. However, bending tests and ESPI provide information on a different length scale compared to nanoindentation.

One means of evaluating which method produces the most accurate results is to take advantage of the correlation between mineral content and elastic modulus in bones from diverse sources [9–11]. We determined the ash mass (ash weight / dry weight * 100) of 3 of the femoral segments frozen for eight months and obtained a value of 63 ± 0.9%. After converting the ash mass (%) to Ca (mg/g) in the bone and inserting the mean value into the regression equation suggested by Currey [11], the elastic modulus obtained was 13.8 GPa. The values we measured using frozen samples are close to this value, indicating that ESPI measurements are accurate. The conversion is based on the atomic weight of calcium (Ca) in the chemical formulas of carbonate hydroxylapitite: the proportion of Ca in carbonated hydroxylapatite is 39.8% so 63% ash mass is 63 g/100 g bone. This corresponds to 63 * 0.398 − 25.1 g / 100 g Ca in the bone which in turn corresponds to 251 mg/g Ca in the bone.

In this study we noted that the elastic moduli of bone segments frozen at −20 °C for a period of eight months were significantly higher compared to those frozen for a brief two week period or tested fresh (Table 1). Despite the general agreement that freezing at −20 °C has little effect on the elastic modulus of bones of different species [23], the effects of freezing on young murine bones has not been studied. Recently, Nazarian et al. [27] compared the effects of freezing and formalin fixation on 16 week old B6 mice vertebrae and long bones. The authors found no difference between the elastic moduli of fresh vs. frozen/fixed samples, using a four point bending method. However, the study examined bones of older mice which were frozen for a two week period as compared to eight months in this study. Although a separate and detailed investigation is warranted, these results point to possible effects of long-term freezing on the elastic modulus of bone and underline the high sensitivity of the ESPI method.

To conclude, The ESPI-based method described here can be used to accurately and precisely measure the effective elastic modulus of mouse cortical bone in compression and when submerged in water. The measurements are thus made under physiologically relevant conditions. Using this technique we can now mechanically test millimeter-sized cortical bone segments in a standard compression test providing an alternative to whole bone bending tests which underestimate the effective elastic modulus of mice long bones. Finally, the high resolution mapping of the mouse genome [35] and the availability of a multitude of genetically altered mouse models have rendered the mouse one of the most studied skeletal systems in bone research and an invaluable tool in the understanding of major bone disease such as osteoporosis [24,25,31]. ESPI can therefore be used in future studies to gain better insights into how specific mutations and treatments may affect the quality of the bone tissue in mice models.

Acknowledgments

We thank Dr. Meir M. Barak, and Prof. John Currey for their helpful input and Dr. Josh Milgram for his technical support. Support for this research was provided by the Kekst Family Center for Medical Genetics at the Weizmann Institute. S. W. is the incumbent of the Dr. Walter and Dr. Trude Burchardt Professorial Chair of Structural Biology.

References

[1] Akhter MP, Cullen DM, Gong G, Recker RR. Bone biomechanical properties in prostaglandin EP1 and EP2 knockout mice. Bone 2001;29:121–5.
[2] Akhter MP, Cullen DM, Pan LC. Bone biomechanical properties in EP4 knockout mice. Calcif Tissue Int 2006;78:357–62.
[3] Akhter MP, Fan Z, Rho JY. Bone intrinsic material properties in three inbred mouse strains. Calcif Tissue Int 2004;75:416–20.
[4] Barak MM, Weiner S, Shahar R. Importance of the integrity of trabecular bone to the relationship between load and deformation of rat femora: an optical metrology study. J Mater Chem 2008;18:3855–64.
[5] Barak MM, Sharir A, Shahar R. Optical metrology methods for mechanical testing of whole bones. Vet J 2008.
[6] Beaupied H, Lespessailles E, Benhamou CL. Evaluation of macrostructural bone biomechanics. Jt Bone Spine 2007;74:233–9.
[7] Brodt MD, Ellis CB, Silva MJ. Growing C57Bl/6 mice increase whole bone mechanical properties by increasing geometric and material properties. J Bone Miner Res 1999;14:2159–66.
[8] Chen Q, Rho JY, Fan Z, Laulederkind SJ, Raghow R. Congenital lack of COX-2 affects mechanical and geometric properties of bone in mice. Calcif Tissue Int 2003;73:387–92.
[9] Currey JD. The design of mineralised hard tissues for their mechanical functions. J Exp Biol 1999;202:3285–94.
[10] Currey JD. Effects of differences in mineralization on the mechanical properties of bone. Philos Trans R Soc Lond B Biol Sci 1984;304:509–18.
[11] Currey JD. What determines the bending strength of compact bone? J Exp Biol 1999;202:2495–503.
[12] Ferguson VL, Ayers RA, Bateman TA, Simske SJ. Bone development and age-related bone loss in male C57BL/6J mice. Bone 2003;33:387–98.
[13] Horton WA. Skeletal development: insights from targeting the mouse genome. Lancet 2003;362:560–9.
[14] Jamsa T, Jalovaara P, Peng Z, Vaananen HK, Tuukkanen J. Comparison of three-point bending test and peripheral quantitative computed tomography analysis in the evaluation of the strength of mouse femur and tibia. Bone 1998;23:155–61.
[15] Jepsen KJ, Akkus OJ, Majeska RJ, Nadeau JH. Hierarchical relationship between bone traits and mechanical properties in inbred mice. Mamm Genome 2003;14:97–104.
[16] Jepsen KJ, Pennington DE, Lee YL, Warman M, Nadeau J. Bone brittleness varies with genetic background in A/J and C57BL/6J inbred mice. J Bone Miner Res 2001;16:1854–62.
[17] Jiao Y, Chiu H, Fan Z, Jiao F, Eckstein EC, Beamer WG, et al. Quantitative trait loci that determine mouse tibial nanoindentation properties in an F2 population derived from C57BL/6J × C3H/HeJ. Calcif Tissue Int 2007;80:383–90.
[18] Karsenty G. Convergence between bone and energy homeostases: leptin regulation of bone mass. Cell Metab 2006;4(5):341–8.
[19] Karsenty G, Wagner EF. Reaching a genetic and molecular understanding of skeletal development. Dev Cell 2002;2:389–406.
[20] Kavukcuoglu NB, Denhardt DT, Guzelsu N, Mann AB. Osteopontin deficiency and aging on nanomechanics of mouse bone. J Biomed Mater Res A 2007;83:136–44.
[21] Lev-Tov Chattah N, Shahar R, Weiner S. Design strategy of minipig molars using electronic speckle pattern interferometry: comparison of deformation under load between the tooth-mandible complex and the isolated tooth. Adv Mat 2008;20.
[22] Liu J, Xu K, Wen G, Guo H, Li S, Wu X, et al. Comparison of the effects of genistein and zoledronic acid on the bone loss in OPG-deficient mice. Bone 2008;42:950–9.
[23] Martin RB, Sharkey NA. Mechanical effects of postmortem changes, preservation, and allograft bone treatments. In: Cowin SC, editor. Bone mechanics handbook. New-York: CRC Press; 2001.
[24] McCauley LK. Transgenic mouse models of metabolic bone disease. Curr Opin Rheumatol 2001;13:316–25.
[25] McLean W, Olsen BR. Mouse models of abnormal skeletal development and homeostasis. Trends Genet 2001;17:S38–43.
[26] Miller LM, Little W, Schirmer A, Sheik F, Busa B, Judex S. Accretion of bone quantity and quality in the developing mouse skeleton. J Bone Miner Res 2007;22:1037–45.
[27] Nazarian A, Hermannsson BJ, Muller J, Zurakowski D, Snyder BD. Effects of tissue preservation on murine bone mechanical properties. J Biomech 2008.
[28] Price C, Herman BC, Lufkin T, Goldman HM, Jepsen KJ. Genetic variation in bone growth patterns defines adult mouse bone fragility. J Bone Miner Res 2005;20:1983–91.
[29] Raum K, Hofmann T, Leguerney I, Saied A, Peyrin F, Vico L, et al. Variations of microstructure, mineral density and tissue elasticity in B6/C3H mice. Bone 2007;41:1017–24.
[30] Rho JY, Pharr GM. Effects of drying on the mechanical properties of bovine femur measured by nanoindentation. J Mater Sci Mater Med 1999;10:485–8.
[31] Rosen CJ, Beamer WG, Donahue LR. Defining the genetics of osteoporosis: using the mouse to understand man. Osteoporos Int 2001;12:803–10.
[32] Schriefer JL, Robling AG, Warden SJ, Fournier AJ, Mason JJ, Turner CH. A comparison of mechanical properties derived from multiple skeletal sites in mice. J Biomech 2005;38:467–75.
[33] Shahar R, Zaslansky P, Barak MM, Friesem AA, Currey JD, Weiner S. Anisotropic Poisson's ratio and compression modulus of cortical bone determined by speckle interferometry. J Biomech 2007;40:252–64.
[34] Sharir A, Barak MM, Shahar R. Whole bone mechanics and mechanical testing. Vet J 2008;177:8–17.
[35] Shifman S, Bell JT, Copley RR, Taylor MS, Williams RW, Mott R, et al. High-resolution single nucleotide polymorphism genetic map of the mouse genome. PLoS Biol 2006;4:e395.

[36] Silva MJ, Brodt MD, Fan Z, Rho JY. Nanoindentation and whole-bone bending estimates of material properties in bones from the senescence accelerated mouse SAMP6. J Biomech 2004;37:1639–46.
[37] Somerville JM, Aspden RM, Armour KE, Armour KJ, Reid DM. Growth of C57BL/6 mice and the material and mechanical properties of cortical bone from the tibia. Calcif Tissue Int 2004;74:469–75.
[38] Tang B, Ngan AH, Lu WW. An improved method for the measurement of mechanical properties of bone by nanoindentation. J Mater Sci Mater Med 2007;18:1875–81.
[39] Torcasio A, van Oosterwyck H, van Lenthe GH. The systematic errors in tissue modulus of murine bones when estimated from three-point bending. J Biomech 2008;41(S1):S14.
[40] Turner CH, Burr DB. Basic biomechanical measurements of bone: a tutorial. Bone 1993;14:595–608.
[41] van Lenthe GH, Voide R, Boyd SK, Muller R. Tissue modulus calculated from beam theory is biased by bone size and geometry: implications for the use of three-point bending tests to determine bone tissue modulus. Bone 2008;43:717–23.
[42] Vashishth D. Small animal bone biomechanics. Bone 2008;43:794–7.
[43] Wergedal JE, Sheng MH, Ackert-Bicknell CL, Beamer WG, Baylink DJ. Genetic variation in femur extrinsic strength in 29 different inbred strains of mice is dependent on variations in femur cross-sectional geometry and bone density. Bone 2005;36:111–22.
[44] Yang L, Zhang P, Liu S, Samala PR, Su M, Yokota H. Measurement of strain distributions in mouse femora with 3D-digital speckle pattern interferometry. Opt Lasers Eng 2007;45:843–51.
[45] Zaslansky P, Currey JD, Friesem AA, Weiner S. Phase shifting speckle interferometry for determination of strain and Young's modulus of mineralized biological materials: a study of tooth dentin compression in water. J Biomed Opt 2005;10:024020.
[46] Zaslansky P, Friesem AA, Weiner S. Structure and mechanical properties of the soft zone separating bulk dentin and enamel in crowns of human teeth: insight into tooth function. J Struct Biol 2006;153:188–99.
[47] Zaslansky P, Shahar R, Friesem AA, Weiner S. Relations between shape, materials properties, and function in biological materials using laser speckle interferometry: in situ tooth deformation. Adv Funct Mat 2006;16:1925–36.